UDK 620.1:669.14.018.8:544.016.5
Original scientific article/Izvirni znanstveni članek

ISSN 1580-2949
MTAEC9, 52(6)835(2018)

DETERMINATION OF THE PHASE-ORIENTATION RELATIONSHIP AND A QUANTITATIVE MICROSTRUCTURE ANALYSIS FOR ASTM A351 STAINLESS STEEL

DOLOČITEV FAZNE ORIENTACIJSKE ODVISNOSTI IN KVANTITATIVNA FAZNA ANALIZA NERJAVNEGA JEKLA ASTM A351

Matjaž Godec[1], Borivoj Šuštaršič[1], Caroline Toffolon-Masclet[2], Bernard Marini[2]

[1]Institute of Metals and Technology, Lepi pot 11, 1000 Ljubljana, Slovenia
[2]Commissariat à l'Energie Atomique, DMN/SRMA, 91191 Gif-sur-Yvette, Saclay, France
matjaz.godec@imt.si

Prejem rokopisa – received: 2018-11-08; sprejem za objavo – accepted for publication: 2018-11-08

doi:10.17222/mit.2018.239

High-alloyed Cr-Ni-based stainless-steel cast alloys are frequently used for the structural parts in conventional and nuclear power plants. The ageing behaviour of cast 258-type stainless steel (ASTM A351) has been studied. The steel samples were isothermally annealed for 10,000 hours at a temperature of 350 °C. Different analytical techniques were used to determine the content of δ-ferrite and the orientation relationship for the austenite solidified on already-formed δ-ferrite. It was also demonstrated that the hardness and ductility changed significantly during ageing due to phenomena associated with spinodal decomposition.

Key words: cast stainless steel, quantitative microstructure characterization, phase-orientation relationship, EBSD (electron backscatter diffraction)

Konstrukcijski deli v konvencionalnih in jedrskih elektrarnah so pogosto izdelani iz močno legiranega Cr-Ni nerjavnega jekla. Raziskali smo staranje nerjavnega jekla tipa 258 (ASTM A351). Vzorce jekla smo izotermno žarili 10.000 ur pri temperaturi 350 °C. Za določanje vsebnosti δ-ferita in orientacijskega razmerja do austenita, strjenega na že formiranem δ-feritu, smo uporabili različne analitske tehnike. Ugotovljeno je bilo tudi, da se trdnost in žilavost med staranjem bistveno spremenita zaradi pojavov, povezanih s spinodalnim razpadom.

Ključne besede: lito nerjavno jeklo, kvantitativna mikrostrukturna karakterizacija, fazna orientacijska odvisnost, metoda EBSD (uklon povratno sipanih elektronov)

1 INTRODUCTION

High-alloyed Cr-Ni-based duplex stainless-steel cast alloys are frequently used for structural parts, for example, as pipes and elbows, in conventional and nuclear power plants.[1,2] These alloys have a characteristic duplex structure consisting of austenite and δ-ferrite.[3] The content of δ-ferrite depends not only on the chemical composition of the alloy but also to a large extent on various metallurgical factors, i.e., the manufacturing procedure and exploitation conditions (time and temperature, maintenance, i.e., repair welding, etc.). Therefore, in the same steel grade, within the allowed ranges of the alloying elements, completely different microstructures can form. This can lead to different mechanical properties of the material and different behaviour during its exploitation.

δ-ferrite is a metastable phase that spinodally decomposes into two phases ($\alpha = \alpha + \alpha'$) with significantly different contents of Cr. This can happen even at relatively low temperatures (approx. 300 °C), which are similar to the operating temperatures of the vital parts of a power plant's coolant system.[2,4–8] The formation of two phases with the same crystal structure but different lattice parameters can cause high internal elastic stresses. This might be one of the reasons for a significant hardness increase and a decrease of the impact toughness. Many years of exploitation of the mechanical equipment in these facilities have shown that the Charpy impact energy of such alloys depends closely on the δ-ferrite content.[9] Therefore, a non-destructive assessment of the δ-ferrite content based on the magnetic induction is a standard checking procedure for the weldments and cast structural elements in thermoelectric installations.[10–12] Previous investigations also showed that the austenite phase does not play a significant role in this process.

The aim of our investigation was to determine the microstructure and to estimate the amount of austenite and δ-ferrite. Furthermore, the orientation relationship of the austenite and δ-ferrite phases was defined by comparing the best fit with one of the well-known orientation relationships between the body-centred cubic (bcc) and face-centred cubic (fcc) crystal structures.[13] Finally, the mechanical testing and scanning electron microscopy

(SEM) fractographic examinations of selected samples were performed.

2 EXPERIMENTAL PART

The samples of Cr-Ni-Mo-based cast alloy (258-type stainless steel) were conventionally melted and centrifugally cast, austenitized for 1 h at 1150 °C, rapidly cooled (water quenched) and then isothermally annealed at 350 °C for 10,000 h.

The actual chemical composition of the investigated alloy was determined with optical- and inductively coupled plasma atomic emission spectroscopy (OES and ICP-AES). The carbon and sulphur contents were determined with infra-red absorption (Eltra CS 800). The nitrogen content was determined with volumetric titrimetry and silicon gravimetrically. All the other elements were determined with ICP-AES (Perkin Elmer Optima 3100 RL). The microstructure investigations were performed with a Nikon MicrophotX light microscope (LM) and a JEOL JSM 6500F field-emission scanning electron microscope (SEM) with energy-dispersive spectroscopy (an INCA X-SIGHT LH2-type detector, INCA ENERGY 450 software) and EBSD (HKL Nordlys II EBSD camera using Channel5 software). Standard preparation procedures (cutting, grinding, polishing) were used for the preparation of the metallographic samples. The microstructure of the examined steel was revealed by etching in potassium hydroxide and potassium ferricyanide. The content of δ-ferrite was determined by using potassium hexacianoferrate at 70 °C for 1 min.

The samples for the SEM/EBSD investigations were fine polished using a silica colloidal suspension with 40-nm particles. For the EDS analysis a 15-kV accelerating voltage and a probe current of 0.9 nA were used and the surface was polished in the same way as for the EBSD analysis. The parameters were chosen because they represent a good compromise between the size of the analyzing volume and the overvoltage needed to detect the chemical elements that are present. EBSD mapping and spot analyses were performed with samples tilted at 70.0° using a 20-kV accelerating voltage and a 1.5-nA probe current. The EBSD map was generated at a step size of 4 μm using 613 × 459 grids with 4 × 4 binning and employing 25 reflectors for the best discrimination between the bcc and fcc phases.

Tensile-test specimens with dimensions of ϕ5 mm × 25 mm were produced from the aged samples and standard tensile tests were performed at room temperature. The SEM fractography of the fractured surfaces was then performed. The microhardness measurements of the δ-ferrite and austenite phases were determined on polished metallographic samples. The tensile testing at room temperature was performed with a 500-kN Instron 1255 testing machine in accordance with SIST EN 10002-1:2002 and DIN 50125:2006. The microhardness measurements were performed with a Fischerscope H100 C nano-indenter.

The individual microstructure constituents were quantitatively defined using several different methods and then compared. The proportions of gamma phase (austenite) and δ-ferrite were estimated using an empirical formula and the CALPHAD (Calculation of Phase Diagrams) based ThermoCalc computer calculation tool. Then the contents of austenite and δ-ferrite were determined by magnetic induction, based on a method using a ferrite meter. In addition, the microstructure constituents were investigated using optical microscopy (LM). The area fraction of each phase was determined using the planimetric method with the image-analysis software analysis 3.1 and a Microphot FXA Nikon light microscope. Twenty fields of view with a size of 1.02 mm^2 were analysed. Last but not least, the proportion of austenite and δ-ferrite was determined using the electron-backscatter diffraction (EBSD) technique, where the amount of each phase was determined crystallographically. Again, twenty fields of view with a size of 4.68 mm^2 were analysed.

In addition, the orientation relationship of the austenite and δ-ferrite phases was defined by comparing the best fit with one of the well-known orientation relationships between the body-centred cubic (bcc) and the face-centred cubic (fcc) crystal structures.[13]

3 RESULTS AND DISCUSSION

3.1 Chemical composition

From the results of the analyses it is clear that any change in the bulk chemistry is negligible with respect to the temperature and the time of ageing. **Table 1** shows the results of the bulk chemical analyses of the investigated alloy, aged at two different temperatures and times (at IMT Ljubljana). This confirms that a change in the bulk chemistry does not occur during ageing, and therefore it cannot be responsible for any change in the mechanical properties of the investigated material. Material in the non-aged condition was also analysed with OES (at CEA, Saclay). It is clear that the two analyses are very similar. The only significant difference

Table 1: The results of ICP-AES bulk average chemical analyses of the investigated alloy

Sample ageing condition	Cr	Ni	Mo	Cu	Mn	Nb	Co	Si	C	S	N	
	w/%											
Non aged	IMT	22.74	9.85	2.35	0.27	0.92	0.27	0.07	0.76	0.040	0.002	0.051
	CEA	22.28	9.92	2.34	0.26	0.91	0.05	0.06	0.86	0.033	0.003	0.051
350°C for 10,000 h	22.78	9.89	2.35	0.27	0.92	0.26	0.07	0.74	0.050	0.002	0.048	

is in the Nb content. Generally, the ICP-AES method is more accurate, while OES demands a special, additional calibration procedure for the Nb content in this type of alloy.

3.2 Determination of the delta ferrite content

The content of δ-ferrite was determined with four different methods: a) calculated with an empirical equation based on the experimentally determined chemical composition (see **Table 1** and Equations (1) and (2)), b) metallographically, c) magnetically, based on the magnetic induction[11] and d) with the SEM/EBSD method.

$$CR = \frac{w(\mathrm{Cr_{eq}})}{w(\mathrm{Ni_{eq}})} = \frac{[w(Cr)+1.5w(Si)+1.4w(Mo)+w(Nb)-4.99]}{[w(Ni)+30w(C)+0.5w(Mn)+26(w(N)-0.02)+2.77]} \quad (1)$$

$$F = -68.768+157.909CR-133.171CR^2+47.1849CR^3 \quad (2)$$

The average content of δ-ferrite was approximately 28 % (x/%), and this does not change significantly with the ageing conditions. **Table 2** shows the results of the δ-ferrite content calculated using Equations (1) and (2).

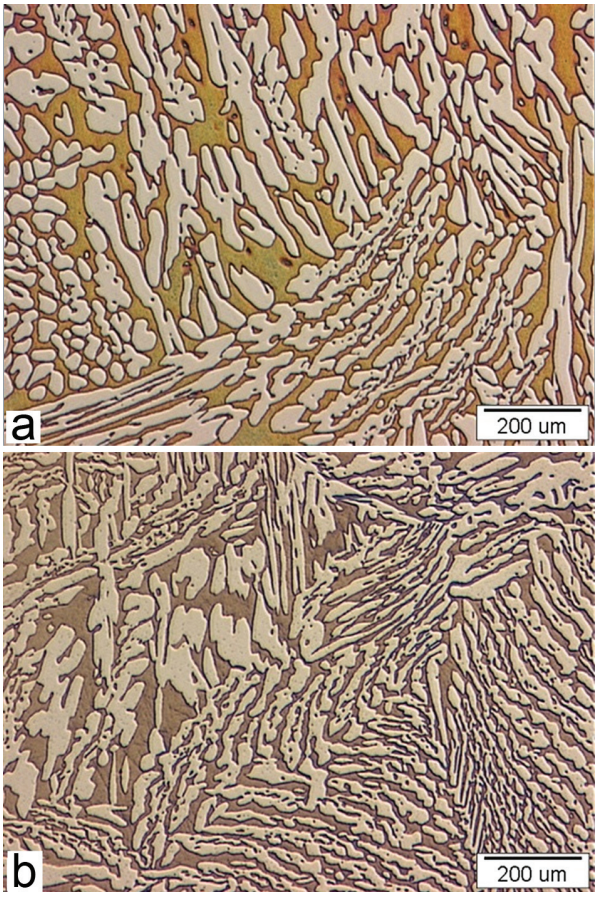

Figure 1: Microstructure of investigated steel, visible under LM: a) non-aged condition and b) material aged at 350 °C for 10,000 h; etched in potassium hexacianoferrate, 70 °C/1 min. δ-ferrite phase is brown and austenite phase is white

This was already proved during systematic investigations of alloys with similar chemical compositions.[14]

Table 2: Average content of δ-ferrite in the investigated cast alloy, calculated with empirical equation taking into account the experimentally determined chemical composition

Sample designation	Cr equivalent	Ni equivalent	δ-ferrite content (x/%)
Base (non-aged) material	22.45	15.09	26.2
350°C for 10,000 h	22.69	15.30	26.4

The microstructures obtained using LM show typical cast dendritic dual-phases (ferrite-austenite) for the investigated material (**Figure 1).** No major difference can be observed between the non-aged and aged conditions at this magnification. The differences can, however, be seen at much higher magnifications, at the nano level, inside the δ-ferrite grains, observed under a high-resolution transmission electron microscope[15] or using atom-probe microscopy[6–8,16] due to the spinodal decomposition.

Different etching agents can be used to reveal the microstructure. However, in order to be able to perform an image analysis it is necessary to discriminate clearly between the two phases, and this is best done by etching in potassium hexacianoferrate, where the δ-ferrite is coloured brown and the austenite is unattached and coloured white. Using standard, semi-automatic image analyses and setting up the appropriate thresholding for the RGB/HSV or greyscale mode of the LM micrographs, the results could be far from what is expected.

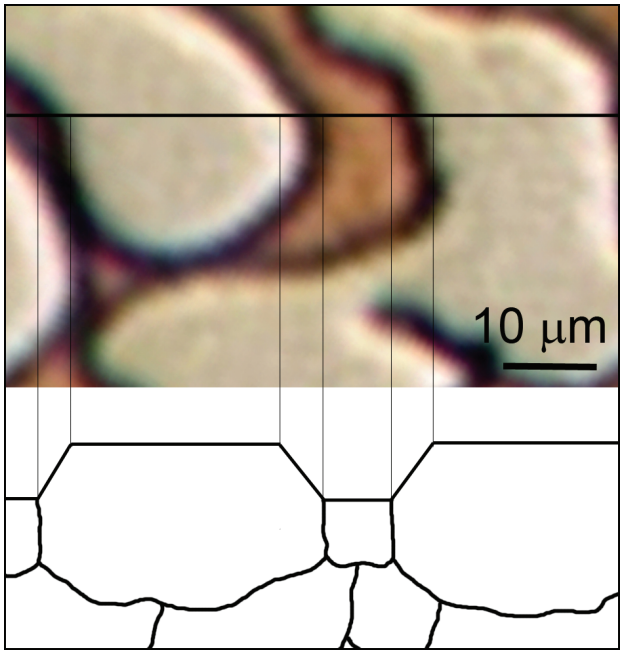

Figure 2: Detail from the microstructure obtained with a light microscope etched in potassium hexacianoferrate with a sketch of the cross-section to explain the overestimated amount of δ-ferrite phase obtained by semi-automatic image analysis

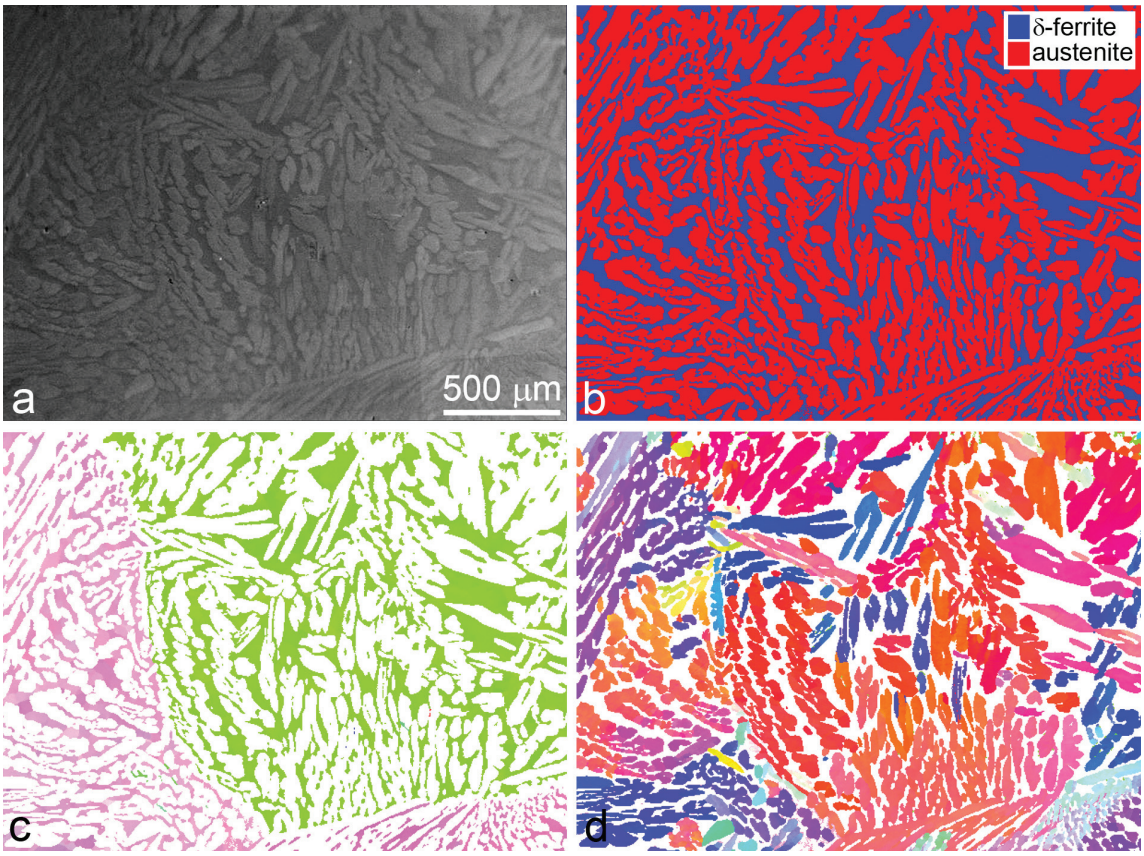

Figure 3: Electron back-scatter diffraction (EBSD) map of base material; a) band-contrast image, b) phase map c) IPF images of δ-ferrite phase and d) IPF images of austenite phase

The δ-ferrite content obtained using the standard procedure was approximately 34–36 %. **Figure 2** might explain the reason for such a large amount of δ-ferrite phase. Etching with potassium hexacianoferrate attacked the δ-ferrite and coloured it brown. The etching needs to be very aggressive in order to obtain the dark ferrite phase and the light austenite phase, causing significant differences in the height topography of the two phases. The consequence of this is a steep wall close to the ferrite-austenite grain boundary. However, when setting the threshold it is very important not to include the dark boundary with the δ-ferrite phase. The amount of phases can vary by a few percent.

The microstructure of the steel samples was also investigated using the EBSD technique. An aged steel sample (350 °C for 10,000 h) is shown in **Figure 3. Figure 3a** shows a band-contrast image, **Figure 3b** presents a phase analysis, while **Figure 3c** and **3d** present IPF images of the δ-ferrite phase and the austenite phase, respectively. The ferrite phase has very large dendrite grains, a few millimetres in diameter, while the austenite grains that grow on the ferrite grains are smaller, in the range 200–500 µm.

The last method used for the phase-content determination is based on the magnetic induction. **Table 3** summarises the results for all the used methods. The lowest values are obtained using an empirical correlation. The results of the semi-automatic image analysis of the LM micrographs give overestimated values for the δ-ferrite content. However, taking into account the phenomena explained in **Figure 2,** the results of the LM image analysis are similar to the others. The results of the magnetic-induction-based method and the SEM/EBSD are also in good agreement with the theoretical ThermoCalc calculation, which gives an equilibrium value for the δ-ferrite content of 32.4 % (x/%) for the 258-type stainless steel austenitized at 1150 °C (**Figure 4**). An EBSD phase analysis is supposed to give the most reliable results. However, there are two conditions that have to be satisfied: it is very important to use the right parameters (number of reflectors, number of bands detected, binning, etc.) to be able discriminate between

Table 3: The comparison of average δ-ferrite contents (x/%), determined with different techniques

Sample designation	Empirical	Magnetic induction	Metallographic method	SEM/EBSD
Base (non-aged) material	26.2	32.4	30.5±2.5	31.4±1.6
350°C for 10,000 h	26.4	29.5	30.2±3.1	29.1±1.7

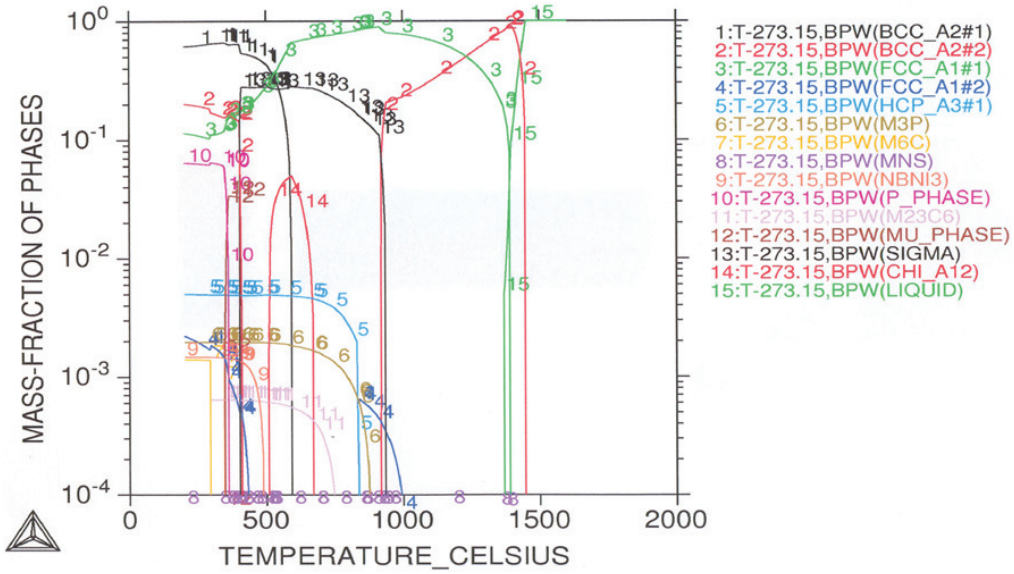

Figure 4: ThermoCalc calculation; equilibrium phase content vs. temperature for 258 type of alloy

the bcc and fcc phases very reliably, and if the microstructure is not very homogenous, then a large area has to be analysed. However, the number of fields examined and the standard deviation obtained give the percentage relative accuracy (for a 95 % confidence interval). For 20 fields a 2.093 confidence interval multiplier was used.[17]

The scanning electron microscopy and area microanalyses (SEM/EDS) of the ferrite and austenite were also performed at different locations on the investigated samples, as shown in **Figures 5a** and 5**b**. Typically, the ferrite is rich in α-genes-forming elements (Cr, Mo, Si) and the austenite is rich in the so-called γ-genes elements (Ni, Mn). The results were compared with the analyses performed at CEA Saclay and are very similar.

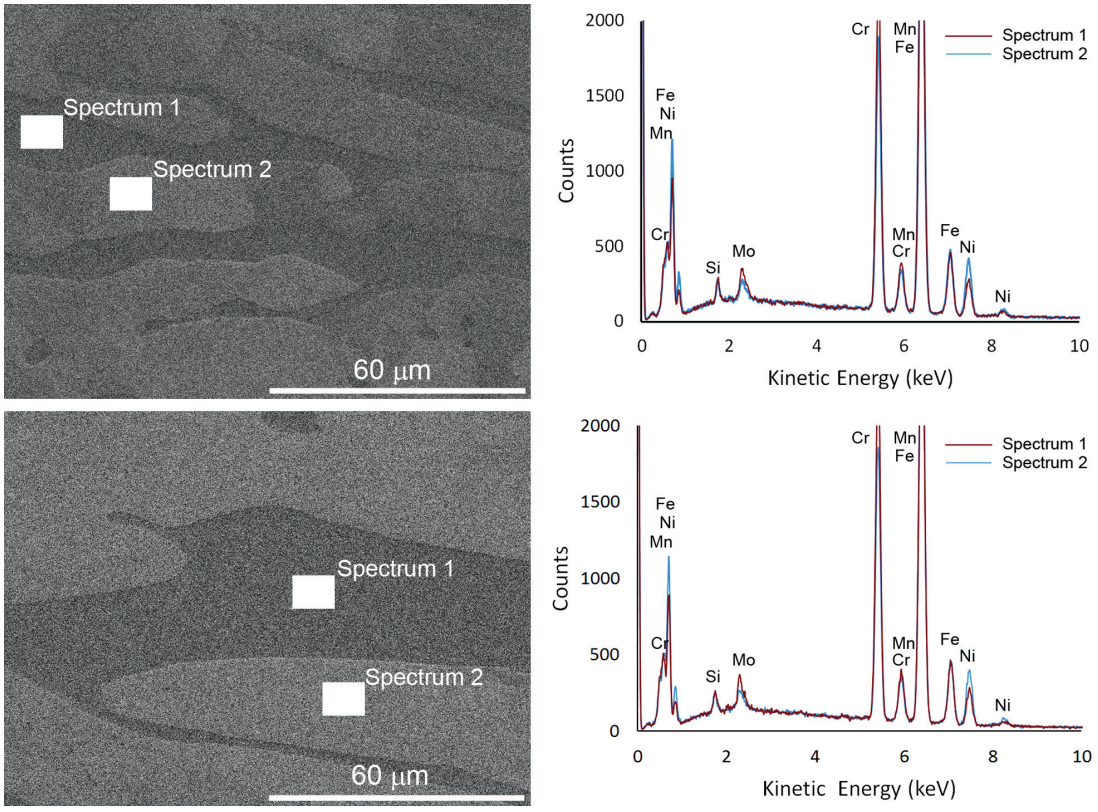

Figure 5: SEI image of analysed surface of selected samples with designated regions, where microchemical analyses were made a) base non-aged material and b) aged material at 350 °C for 10,000 h

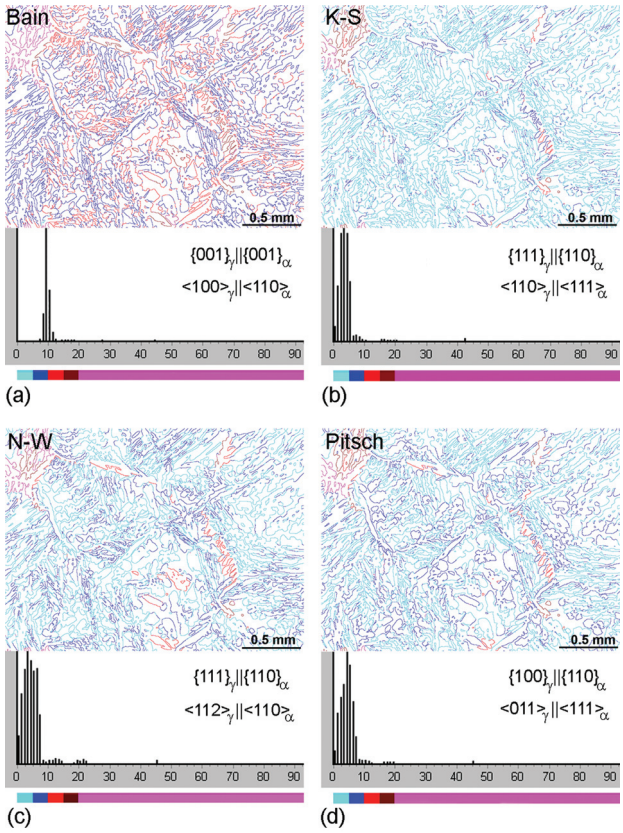

Figure 6: Orientation relationship boundaries of δ-ferrite and austenite phase to one of the well-known orientation relationships. The best match is closest to zero degrees in this case for the Kordjumov-Sachs orientation relationship.

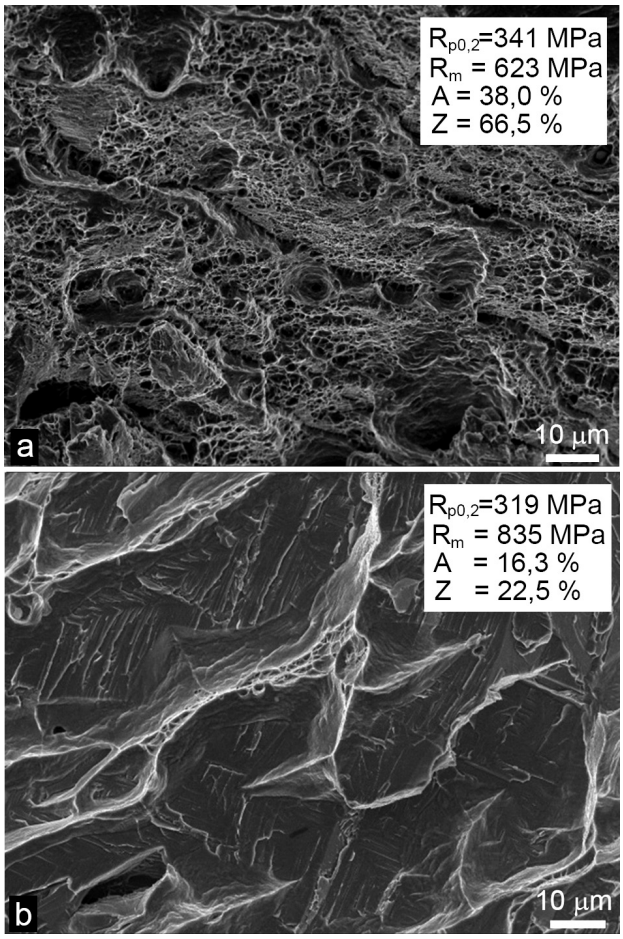

Figure 7: SE image fractographies of investigated material, surface of broken tensile test specimens with some results of mechanical tests: a) base material, b) aged at 350 °C for 10,000 h

3.3 Phase orientation

The SEM/EBSD method was also used to determine the orientation relationship of the austenite and δ-ferrite phases by comparing the best fit of the well-known orientation relationships for the bcc and fcc crystal structures. It was found that the austenite phase grows in a certain orientation relationship with respect to the δ-ferrite. The orientation relationship boundaries of the δ-ferrite and the austenite phase with respect to one of the well-known orientation relationships, i.e., Bain, Kordjumov-Sachs, Nishiiama-Wassermann and Pitsch,[13] are shown in **Figure 6**. The light-blue grain boundaries represent the best fit and show that the austenite solidifies on the already-formed δ-ferrite in the Kordjumov-Sachs orientation relationship. The densest plane {111} of the austenite is parallel to the densest plane {110} of the δ-ferrite and the n direction in the austenite is parallel to the o direction in the δ-ferrite, and this is the well-known Kordjumov-Sachs orientation relationship.[13]

3.4 Mechanical testing

The yield point $R_{p0.2}$, the tensile strength R_m, the elongation A and the contraction of the area Z were determined. A fractographic examination of broken tensile-test specimens was made with the SEM. An ageing time of 10,000 h and a temperature of 350 °C cause structural changes, which result in a deterioration of the mechanical properties. While the yield point and the tensile strength increase, the ductility dramatically decreases. This is also evident from the SEM fractographic examination. In accordance with the ductility decrease, the nature of the fracture surface changed from typical ductile (dimpled) (**Figures 7a**, to brittle (cleavage) (**Figures 7b**). The microhardness of the initial austenite is 2.58 GPa and remains almost the same during ageing, which is 2.65 Gpa, while the microhardness of the initial δ-ferrite is 4.1 GPa and increases during ageing to 8.3 GPa. The microhardness measurements proved that for this overall change of the mechanical properties it is nanostructural changes in the δ-ferrite that are responsible. The microhardness of the austenite is practically unchanged, but with a prolonged ageing time and an increased temperature the microhardness of the ferrite increases significantly.

4 CONCLUSIONS

The bulk chemical analyses of a non-aged and an aged cast alloy were performed at IMT, Ljubljana, Slovenia and CEA, Saclay, France. The results of the analyses are in good agreement and clearly show that the change of the bulk chemistry is negligible with the temperature and time of ageing.

The content of δ-ferrite before and after ageing was determined with four different methods and remains the same, if we take into account the measurement uncertainty and the fact that the material is not absolutely homogeneous. Based on an empirical correlation the fraction of δ-ferrite was estimated to be 26.2 % (after ageing 26.4 %), the magnetic-induction-based method gave 32.4 % (after ageing 29.5 %), the metallographic method, 30.5 % (after ageing 30.2 %) and the EBSD phase analysis, 31.4 % (after ageing 29.1 %). The closest and the most reliable results were obtained with magnetic-induction and SEM/EBSD methods, as long as certain parameters are well defined. The semi-automatic image analysis of the LM micrographs provided values of the δ-ferrite content that were too large, because of over-etching of the ferrite-austenite grain boundaries. However, when taking into account this phenomenon, the results can be very precise. The results of the magnetic-induction-based method and the SEM/EBSD correlate well with the theoretical Thermo-Calc calculations. Austenite and δ-ferrite are in a Kordjumov-Sachs orientation relationship, where the densest plane {111} of the austenite is parallel to the densest plane {110} of the δ-ferrite and the *n* direction in the austenite is parallel to the *o* direction in the δ-ferrite. The ferrite phase has very large dendrite grains, a few millimetres in diameter, while the austenite grains that grow on the ferrite grains are smaller and in the range 200–500 μm.

Finally, the mechanical testing and SEM fractographic examinations of selected samples were performed. The microhardness of the ferrite is drastically increased with the time and temperature of ageing due to the spinodal decomposition. However, the hardness of the austenite remains practically unchanged. The tensile properties changed in a similar way. The yield point and the tensile strength increased, but the ductility decreased significantly. In accordance with the ductility decrease the nature of the fracture surface changed from typical ductile to brittle, and from dimpled to cleavage, respectively.

Acknowledgment

The authors wish to thank the Slovenian Research Agency, as well as the French Atomic Agency, for their financial support.

5 REFERENCES

[1] J. K. Sahu, U. Krupp, R. N. Ghosh, H.-J. Christ, Effect of 475 °C embrittlement on the mechanical properties of duplex stainless steel, Mater. Sci. Eng. A, 508 (**2009**), 1–14, doi:10.1016/j.msea.2009.01.039

[2] H. M. Chung, Aging and life prediction of cast duplex stainless steel components, Int. J. Press. Vessel. Pip., 50 (**1992**), 179–213, doi:10.1016/0308-0161(92)90037-G

[3] M. Vasudevan, A. K. Bhaduri, B. Raj, K. P. Rao, Delta ferrite prediction in stainless steel welds using neural network analysis and comparison with other prediction methods, J. Mater. Process. Technol., 142 (**2003**), 20–28, doi:10.1016/S0924-0136(03)00430-8

[4] F. Danoix, P. Auger, Atom probe studies of the Fe–Cr System and stainless steels aged at intermediate temperature: A review, Mater. Charact., 44 (**2000**), 177–201, doi:10.1016/S1044-5803(99)00048-0

[5] K. L. Weng, H. R. Chen, J. R. Yang, The low-temperature aging embrittlement in a 2205 duplex stainless steel, Mater. Sci. Eng. A, 379 (**2004**), 119–132, doi:10.1016/j.msea.2003.12.051

[6] J. D. Tucker, M. K. Miller, G. A. Young, Assessment of thermal embrittlement in duplex stainless steels 2003 and 2205 for nuclear power applications, Acta Mater., 87 (**2015**), 15–24, doi:10.1016/j.actamat.2014.12.012

[7] S. Li, T. Wang, Q. Tan, R. Li, Y. Wang, X. Wang, Y. Ren, Y. Wang, A brittle fracture mechanism in thermally aged duplex stainless steels revealed by in situ high-energy X-ray diffraction, Mater. Sci. Eng. A, 739 (**2019**), 264–271, doi:10.1016/j.msea.2018.10.025

[8] S. Mburu, R. P. Kolli, D. E. Perea, S. C. Schwarm, A. Eaton, J. Liu, S. Patel, J. Bartrand, S. Ankem, Effect of aging temperature on phase decomposition and mechanical properties in cast duplex stainless steels, Mater. Sci. Eng. A, 690 (**2017**), 365–377, doi:10.1016/j.msea.2017.03.011

[9] F. Xue, Z.-X. Wang, G. Shu, W. Yu, H.-J. Shi, W. Ti, Thermal aging effect on Z3CN20.09M Cast Duplex Stainless Steel, Nucl. Eng. Des., 239 (**2009**), 2217–2223, doi:10.1016/j.nucengdes.2009.06.009

[10] EN ISO 13520:2015 Determination of ferrite content in austenitic stainless steel castings, ISO – International Organization for Standardization, Geneve

[11] EN ISO 8249:2018 s Welding – determination of ferrite number (FN) in austenitic and duplex ferritic-austenitic Cr-Ni stainless steel weld metals, ISO – International Organization for Standardization, Geneve

[12] ASTM A800 / A800M-01:2006 Standard Practice for Steel Casting, Austenitic Alloy, Estimating Ferrite Content Thereof, ASTM International, West Conshohocken (Pennsylvania)

[13] Y. He, S. Godet, J. J. Jonas, Representation of misorientations in Rodrigues-Frank space: Application to the Bain, Kurdjumov-Sachs, Nishiyama-Wassermann and Pitsch orientation relationships in the Gibeon meteorite, Acta Mater., 53 (**2005**), 1179–1190, doi:10.1016/j.actamat.2004.11.021

[14] B. Sustarsic, B. Podmiljsak, P. McGuiness, J. V. Tuma, Magnetic characteristics of isothermally aged Cr-Ni-Mo-based alloys with different delta-ferrite contents, Mater. Tehnol., 43 (**2009**), 129–135

[15] J. E. Westraadt, E. J. Olivier, J. H. Neethling, P. Hedström, J. Odqvist, X. Xu, A. Steuwer, A high-resolution analytical scanning transmission electron microscopy study of the early stages of spinodal decomposition in binary Fe–Cr, Mater. Charact., 109 (**2015**), 216–221, doi:10.1016/j.matchar.2015.10.001

[16] U. Krupp, M. Söker, A. Giertler, B. Dönges, H.-J. Christ, K. Wackermann, T. Boll, M. Thuvander, M. C. Marinelli, The potential of spinodal ferrite decomposition for increasing the very high cycle fatigue strength of duplex stainless steel, Int. J. Fatigue, 93 (**2016**), 363–371, doi:10.1016/j.ijfatigue.2016.05.012

[17] ASTM E562-11:2011 Standard test method for determining volume fraction by systematic manual point count, ASTM International, West Conshohocken (Pennsylvania)